Optical Review (2020) 27:225–232
https://doi.org/10.1007/s10043-020-00581-0

SPECIAL SECTION: REGULAR PAPER

The 13th Japan-Finland Joint Symposium on Optics in Engineering (OIE'19), Espoo, Finland and Tallinn, Estonia

Predicting scattering properties of fiber suspensions using Mie theory and probabilistic cross-sectional diameter of fibers

Harri J. Juttula[1] · Matti Törmänen[2] · Anssi J. Mäkynen[3]

Received: 27 September 2019 / Accepted: 13 January 2020 / Published online: 6 February 2020

Abstract
Scattering of visible light by micrometer-scale natural wood fibers is usually treated by assuming fibers to be perfect long cylindrical scatterers. In industrial processes, however, fibers experience deformations and are far from ideal cylinders. Variation in fiber morphology affects their scattering properties and it poses a challenge for reliable process measurements. In this paper, we have studied experimentally scattering of both deformed natural and ideal artificial non-absorbing fibers in aqueous suspension and their response to mass concentration of fibers. Experimental results are compared with the predictions of the Mie theory which is combined with cross-sectional diameter probability distribution of fibers. It is shown that the diameter distribution of the fibers together with Mie theory provides results that agree with experiments in case of both natural and ideal fibers.

Keywords Scattering · Mie · Paper pulp · Consistency

1 Introduction

In the paper and board industry, the requirements for higher paper quality, the more effective use of raw materials, and higher processing speed need new measurement methods and tools. Paper and paperboard are made of paper machine furnish, which consists of water suspended mixture of paper pulp and various additives. Paper pulp consists of cellulose fibers extracted from trees, while additives may include dyes and inorganic fillers like kaolin, calcium carbonate, talc, or titanium dioxide, for example. Cellulose fibers provide the basic structure and strength for the paper and fillers are mainly used to improve the appearance and printing properties as well as to increase the grammage (thickness) of the paper.

One of the most important control parameters of paper making is the total mass fraction, or total consistency, of the furnish. It is defined as the mass percentage of all dry material (fibers and fillers) of the furnish. Today, there are a number of commercial online instruments, which measure the total mass fraction. Methods used include attenuation and scattering of optical signals [1], attenuation and retardation of microwaves [2, 3], and changes in viscosity of the flowing pulp [4].

Besides the total mass fraction, modern paper-making processes need online information about the mass fractions of fibers and fillers separately. Some experimental optical methods are capable of providing the fiber and the filler mass fractions separately, but may not be practical for industrial use [5, 6]. On the other hand, attempts have been made to calibrate the existing instrumentation to provide separate signals proportional to the fiber and filler mass fractions. Although calibration may be successful for certain fiber and filler combinations, they provide erroneous results if the fiber morphology changes in the process. Thus, wide variation in fiber and filler materials makes this kind of approach very complex and difficult to carry out reliably. Optical

✉ Harri J. Juttula
harri.juttula@oulu.fi

[1] Unit of Measurement Technology, University of Oulu, P.O.Box 127, 87400 Kajaani, Finland

[2] Valmet Automation Inc., Elektroniikkatie 9, 90590 Oulu, Finland

[3] Optoelectronics and Measurement Techniques Unit, University of Oulu, P.O.Box 4500, 90014 Oulu, Finland

methods, for example, may provide widely different results depending on fiber physical dimensions, fibrillation, and the amount of fiber fines. One possible solution would be to analyse the shape parameters of the fibers and the amount of fines using onsite microscopic techniques and then resolve their effect on the response of optical mass fraction sensors using precise optical modelling based on the shape information. Workflow of this approach is described in Fig. 1. This paper studies the necessary preconditions for this kind of approach by comparing the scattering properties of ideal and real (deformed) fiber shapes and their scattering response as a function of mass fraction.

Natural fibers interact with light usually via elastic scattering and absorption. Without any size restrictions, interaction can be modelled using Mie theory and assuming that scattering particles have ideal spherical or cylindrical shape. Natural fibers are, however, far from ideal cylinders and simple cylindrical scattering models do not explain the scattering properties of single fibers. It has been demonstrated that for a single fiber, for example, a gaussian random cylinder model combined with ray-optic approximation explains angular scattering behaviour from natural wood fibers better than scattering theory with ideal cylinder approximation [7]. Despite the shape restriction of the Mie theory, it has been widely applied in many fields. Perhaps, the most common application is particle-size analysis with laser diffraction [8] which typically assumes the particles to be either spherical or cylindrical and requires the scattering events to be independent of each other. In the multiple scattering regime, some examples are, for example, modelling of light propagation in muscle tissue [9, 10] or wood fibers in suspensions or on finished paper [11, 12].

In this work, we have measured the reduced scattering coefficients of artificial ideal cylindrical and deformed natural fibers and compared the results with the Mie scattering theory. Deformations in this context may include for example bending, flattening, or kinking of fibers compared with a perfect cylinder. We will show that both ideal and deformed fiber shapes produce scattering that is directly proportional to the mass fraction of fibers, and if the statistical distributions of the fiber diameters are known, Mie theory reproduces the measured scattering values in excellent manner in both cases. Latter observation has practical importance for mass fraction measurements when the variation in fiber diameter needs to be compensated, since, according to our results, Mie theory can be confidently applied regardless of the shape deformations. This opens a strategy to use simple morphological information of the fibers to connect simple optical scattering-based measurement results to true total mass fraction without furnish specific black-box calibrations. Modern paper mills have laboratory instrumentation for morphological measurements of fibers for quality-control purposes, but, to our knowledge, these have never been used to improve optical process measurements as we propose.

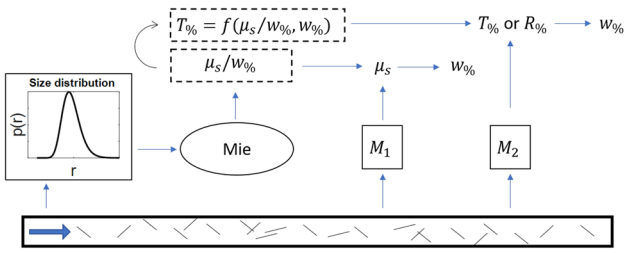

Fig. 1 Principle of utilizing Mie scattering modelling based on fiber size information to derive fiber mass concentration $w_{\%}$ from the measured optical parameters. Currently, optical instruments measure scattering coefficient μ_s either directly (M_1) or indirectly with transmission $T_{\%}$ or reflection $R_{\%}$ of light (M_2). Usually, tedious black-box calibrations with multiple furnish samples are needed to find the relations depicted in the dashed boxes

2 Methods

2.1 Mie theory

Scattering coefficient of a particle suspension can be estimated with the Mie theory if the complex refractive indexes of scattering particles and surrounding medium are known and if the particle sizes are in the Mie scattering regime. Mie scattering regime can be loosely defined as a range where the wavelength of incident light and particle size are close to each other. However, the Mie theory is applicable for a much wider range of particle sizes, and in the visible wavelengths, the typical scattering dimensions of fibers, 10–40 μm, can be treated with the Mie theory [13, 14]. Mie theory provides an analytical solution for simple spherical or infinitely long cylindrical particles with homogeneous or stratified refractive index. Hence, scattering particles are often approximated with either spheres or cylinders. For much more complex shapes or aggregates of particles, there are others methods to treat scattering such as discrete dipole approximation [15, 16] or T-matrix method [17].

In this work, we used the Mie theory to estimate the reduced scattering coefficient μ_s' of natural and artificial fibers by assuming them to be ideal cylinders and using their measured diameter distribution to calculate scattering cross section for ensembles of fibers. Mie calculations in this work are based on the formulations as presented by Bohren and Huffman [13]. In practice, we used a Matlab implementation of the Mie solutions for ideal spheres and infinite cylinders by Schäfer [18, 19]. For cylindrical particles, this allowed us to calculate absorption and scattering cross sections σ_a and σ_s as a function of fiber radius r, relative refractive index n_{rel}, wavelength, and incidence angle between light and cylinder axis ζ. Scattering coefficient of the bulk fiber suspension can

be calculated as a product of the particle number density and the expected value of the scattering cross section averaged over all possible size and orientation probabilities:

$$\langle \mu_s \rangle = \rho_N \int p(r)p(\zeta)\sigma_s(r, n_{rel}, \lambda, \zeta)\mathrm{d}r\mathrm{d}\zeta. \quad (1)$$

Here, ρ_N is the number density of the fibers in mm^{-3}, and $p(r)$ and $p(\zeta)$ are the probability density functions of fiber radius and orientation, respectively. Angle ζ is the orientation angle, and it is defined as angle between the incident light and the axis of the cylinder.

2.2 Measurement setup

A closed loop circulation system was used to measure fiber samples in aqueous suspensions between 0.1 and 1% mass concentrations. Setup consisted of a pump and two independent scattering coefficient measurements: a single wavelength laser backscattering instrument and a total reflectance and transmittance-based measurement with double integrating spheres. Pump and the devices were connected with 1 cm-wide tubes.

Integrating spheres were used to determine absorption and reduced scattering coefficient of the sample suspensions. Sphere setup consisted of halogen light source, two barium sulfate ($BaSO_4$) coated 210 mm diameter integrating spheres with 25 mm sample ports, 2 mm-thick flow through cuvette with 25 mm windows (cuvette 1 in Fig. 2) and Avantes AvaSpec-2048 dual-channel spectrophotometer. This setup was used to measured transmittance and reflectance values which were transformed in post-processing into absorption and reduced scattering coefficients with inverse adding doubling (IAD) program [20, 21]. We will refer to this measurement as the IAD method.

Independent reference measurements from the same flow were performed with single wavelength laser backscattering instrument which was connected to a windowed cylindrical chamber with 10 cm diameter and height (cuvette 2 in Fig. 2). Backscattering instrument consisted of a 660 nm diode laser with a 45° angle of incidence with the sample surface and a high dynamic range (HDR) camera system normal to the measurement surface. Oblique laser angle results in an asymmetrical backscattering pattern which is imaged with HDR camera and the analysis of the shape of backscattering pattern provides values for the absorption and scattering coefficients of the sample suspension. Details of the device and the measurement principle have been reported elsewhere [22]. With this setup, the low-intensity part of the HDR images consists of purely diffuse light that has the axis of symmetry shifted by distance Δx from the point of incidence of laser and it is related to the diffusion coefficient D of the sample by relation:

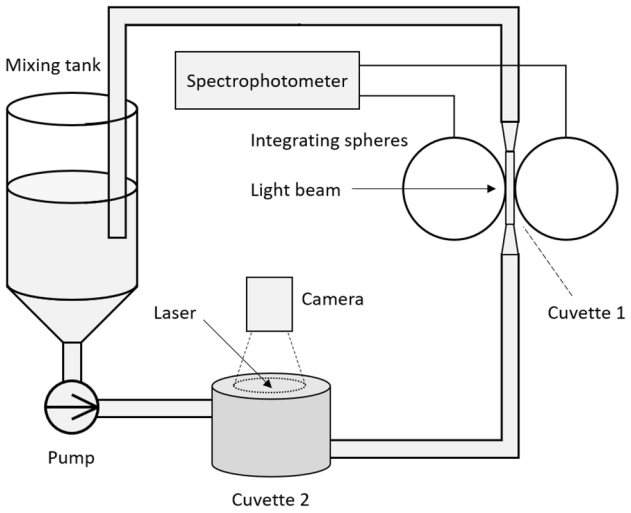

Fig. 2 Measurement setup for closed loop circulation of sample suspension with two independent measurement devices for determination of the scattering coefficient: total transmittance and reflectance based IAD method (cuvette 1) and laser backscattering method (cuvette 2)

$$\Delta x = 3Dsin(\theta_t), \quad (2)$$

where θ_t is transmitted beam angle according to Snell's law. Diffusion coefficient can be further used to solve the reduced scattering coefficient μ_s' and absorption coefficient μ_a [23]:

$$\mu_a = D\mu_{eff}^2 \quad (3)$$

$$\mu_s' = (3D)^{-1} - \mu_a. \quad (4)$$

Here, μ_{eff} is the effective attenuation coefficient which can be measured from the backscattering image, since far away from the point of incidence decay of the intensity is proportional to $exp(-\mu_{eff}r)$. Equations (2)–(4) assume semi-infinite sample space. This condition is fulfilled in our experiments, since the dimensions of the measurement cuvette 2 are larger than the detected photon distribution of backscattered light.

2.3 Samples

Sample materials used in this work were natural wood fibers and artificial rayon fibers. Wood fibers were chemically separated and bleached Nordic pine (NP) fibers from a paper mill. Typical wood fibers are hollow cylinder-like cells which are mainly composed of cellulose, hemicellulose, and lignin. Hollow center (lumen) can be filled with air or water. Bleaching is used to remove lignin and other absorbing components from the fibers, and in the visible wavelengths, scattering becomes the dominant interaction with light ($\mu_s' \gg \mu_a$). The mean diameter of wood fibers depends on species and the separation process, but it is

typically in the order of 20 μm, while the length of the fibers can be as much as 1–3 mm. Rayon, also known as viscose, fibers are artificially manufactured fibers composed of cellulose from natural sources. Rayon fibers (MiniFIBERS inc.) had nominal diameter and length of 10 μm and 2 mm, respectively. Microscope images of both pine and rayon fibers are shown in Fig. 3. From the microscope images, it can be observed that due to separation and bleaching processing, the natural NP fibers resemble more flattened and twisted cylinders, while the artificial rayon fibers are nearly perfect cylinders. Since the pine fibers were mostly flattened, we estimated their density to be 1.55 g/cm^3 which corresponds to the density of the fiber wall rather than the density of hollow wood cells. Similar density was used for rayon material. Densities were needed to transform the particle number density used by the Mie calculations into mass concentrations.

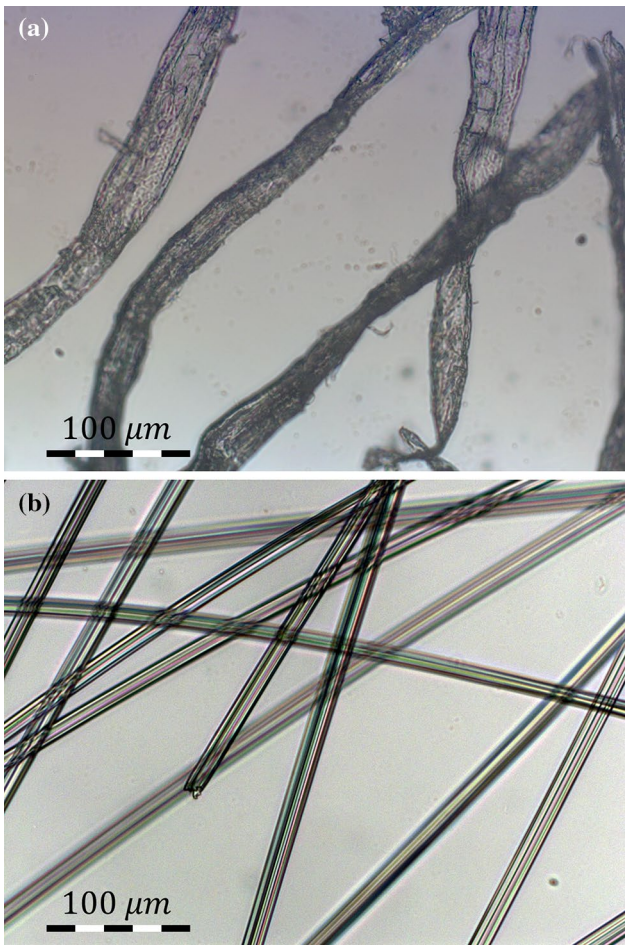

Fig. 3 Microscope images of bleached nordic pine (**a**) and artificial rayon fibers (**b**)

3 Experiments

Both rayon and the NP fibers were measured in aqueous solutions and their mass concentrations were swept between 0.1 and 1%. The upper and lower limits were set by the pumping and measurement capabilities of our measurement setup. Process values for fiber suspensions are typically in the range of 0–4%.

Suspensions were measured by starting from the low mass concentration and gradually increasing it by adding known amount of fibers in the circulation. After each increment suspension was allowed to stabilize for a few minutes and the procedure was continued until the sample viscosity caused the system to clog approximately at 1% mass concentration. At the start of each experiment system was filled with water and carefully de-aired to prevent scattering due to air bubbles.

To determine the μ_s' with the IAD method, normalized reflectance M_R and transmittance M_T were measured with spectrophotometer connected to the integrating spheres. Measurements were performed as an average of 30 individual measurements with 3 s integration times to minimize the effects of local inhomogeneities of the samples which, after averaging, caused less than 1% measurement uncertainty. Normalized M_R and M_T are defined as:

$$M_R = \left(\frac{R_{meas} - R_0}{R_{100} - R_0} \right) r_{std} \tag{5}$$

$$M_T = \left(\frac{T_{meas} - T_0}{T_{100} - T_0} \right). \tag{6}$$

Here, subscripts `0' and `100' refer to minimum and maximum calibration measurements and `meas' refers to raw measurement signal. A diffuse spectralon reflectance standard from LabSphere with known r_{std} was used as reference in calibration. Value of R_{100} was recorded by inserting the reflectance standard in the sample port. R_0 was also measured with light source on but without the second sphere in dark room. This provides a dark reference that accounts for stray light from the collimated light source that misses the sample port and is collected by the first sphere. T_{100} was measured as transmission with empty sample port and T_0 was the dark reference with light source off. Details of the calibration procedure can be found in the manual of the IAD program [21].

Images of the backscattered laser were measured by fusing images with 1 s, 100 ms, 10 ms, and 1 ms exposure times into one HDR image. Backscattered light patterns were measured for each mass concentration and averaged over ten images. Typical resulting HDR image is shown in Fig. 4 in logarithmic intensity scale. From the image asymmetrical backscattering can be observed near the

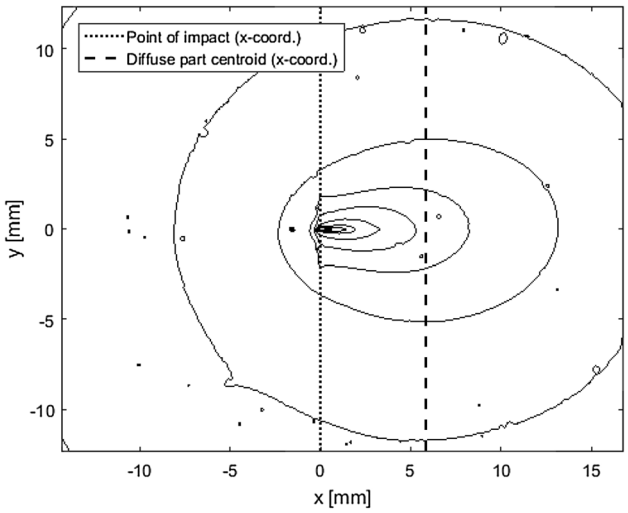

Fig. 4 Log-scale contour plot of the intensity of the backscattered laser light from the fiber suspension sample. Dashed lines mark the point of incidence and the centroid of the diffuse part of backscattered light

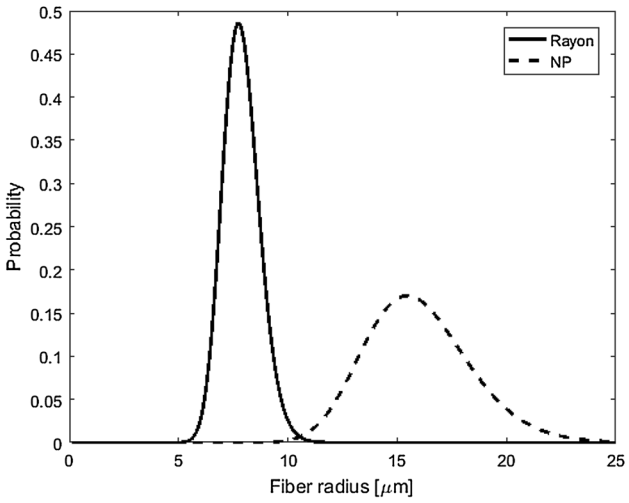

Fig. 5 Lognormal size distribution of the sample fibers. Mean and standard deviation [μ and σ in Eq. (7)] for the distributions were 2.06 and 0.11 for rayon and 2.76 and 0.15 for NP fibers, respectively

point of incidence at origin which transforms into nearly symmetrical diffuse light at lower intensity levels. From each image, location of point of incidence of laser and the centroid of low-intensity diffuse light were measured whose x-coordinates are marked with dashed lines in Fig. 4. Difference of these x-coordinate values is the Δx in Eq. (2).

Reduced scattering coefficient calculations with Mie theory were based on radial size distribution of the fibers. Radial distributions were determined from microscope images with 20× magnification. Two hundred sample radii were measured from the microscope images with ImageJ software (National Institute of Health, USA). We assumed the size distribution to be lognormal and the results were fitted into a probability distribution function:

$$p(r) = \frac{1}{r\sigma\sqrt{2\pi}} exp \frac{-(\ln(r) - \mu)}{2\sigma^2}. \tag{7}$$

Measured radii distributions are shown in Fig. 5. Rayon fibers were nearly perfect cylinders in all the microscope images with a mean radius of 7.83 μm with a narrow size distribution. NP fibers, on the other hand, were observed to be flattened and crooked. Measured radius had mean value of 17.8 μm with a much wider distribution than rayon. Measured radii of NP fibers are actually the radii of 2D projections of flattened cylinders with a random orientation. Since both measurement devices in Fig. 2 measure large amount of fibers during experiments, this probabilistic presentation of radius is reasonable way to solve scattering coefficient with Eq. (1).

4 Results and discussion

We calculated Mie solution for the scattering cross sections of infinitely long cylinders over the observed radius range of the fiber samples and for all possible fiber orientation angles with (1). Refractive indices of water, pine, and rayon used in the Mie calculations were 1.331, 1.555, and 1.47, respectively [24–26]. For rayon, we used the refractive index of cellulose. Results for the Mie solutions are shown in Table 1 together with the scattering coefficients measured by laser backscattering and IAD methods. For $p(r)$, we used the measured size distributions, as shown in Fig. 5, and we assumed isotropical angular distribution $p(\zeta)$ of the fibers. Number density ρ_N of fibers were estimated from the known densities and mass concentrations used in the measurements with the aid of radial distributions of the fibers. Length of the fibers was not required as it cancels out when solving Eq. (1).

Orientation distribution $p(\zeta)$ of the fibers needs to be considered since, according to the Mie theory, scattering coefficient depends on the angle ζ. For example, solution of Eq. (1) may increase by a factor of 2 if the fiber axes are oriented in a plane perpendicular to the incident light if compared to fibers with isotropic orientation distribution. We assumed the orientation distribution $p(\zeta)$ of the fibers to be isotropic in our experiments. This was certainly true in the laser backscattering measurement, since the measurement signal was acquired from a very large and turbulent flow in cuvette 2. IAD method, however, probes a narrow 2 mm-thick flow volume from cuvette 1 where orientation might affect the measurements. We concluded that in our

experiments, orientation of the fibers is not present, since both measurement methods showed similar results.

Measured scattering coefficients of both IAD and laser backscattering methods as a function of mass concentration are shown in Fig. 6. Absorption coefficient of the samples at visible spectrum was below detection capabilities of the instruments. IAD method suffered some convergence issues, since the amount of absorption and scattering interaction was relatively low. This was solved by forcing the IAD program to use 0 for absorption coefficient which was assumed to be a reasonable approximation, since for white rayon and NP fibers, absorption is very small and $\mu_a \ll \mu_s'$ for the visible wavelengths. Although the laser backscattering instrument was able to measure all the samples, it showed more measurement noise due to slow flow speed in cuvette 2. Overall, both methods are in a very good agreement with each other and show linear relation to mass concentration $w_{\%}$ as expected. Agreement of the two methods is important, since it shows that our assumption of isotropic fiber orientation holds true for both measurement cuvettes.

Linear regression model was fitted to the scattering coefficient data. Fit provided us with concentration specific reduced scattering coefficients $\mu_s'/w_{\%}$ with 2σ confidence intervals. Results are collected into Table 1 together with the estimates from the Mie calculations. Mie values calculated from microscope images are close to the measured values for both NP and rayon fibers. Confidence interval for Mie values was estimated by using upper and lower limits of 2σ confidence interval of the measured size distributions.

Table 1 Measured reduced scattering coefficient per mass concentration for fibers in aqueous suspension

	$\mu_s'/w_{\%}$ [mm^{-1}] $\pm 2\sigma$	
	NP	Rayon
IAD	0.044 ± 13%	0.076 ± 15%
Laser backscattering	0.050 ± 27%	0.072 ± 18%
Mie	0.043 ± 11%	0.090 ± 3%

In addition, reduced scattering coefficient per mass concentration of NP fibers was determined spectrally with IAD method. The measured wavelength dependence is shown in Fig. 7 together with error estimates and estimates from Mie calculations. The measured results show scattering coefficient to increase approximately 50% when the wavelength is decreased from 900 to 500 nm. Measured values shown in Table 1 and in Fig. 7 are similar to values presented in [27] for paper furnish. However, Mie calculations predict nearly constant scattering for such a short-wavelength range. It is likely that the spectral behaviour observed with IAD method is mainly due to absorption by cellulose and the spectral transmittance losses of the sapphire windows of the cuvette. If these effects are present, they will be observed as scattering, since we used the no absorption condition in the IAD calculations. It should be noted that below the measured wavelength range absorption of the NP fibers cannot

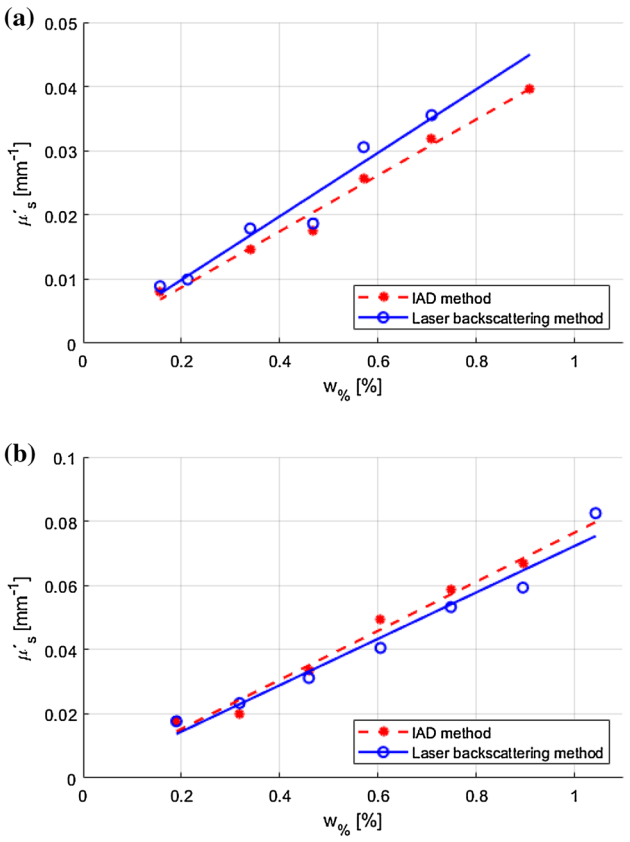

Fig. 6 Reduced scattering coefficients of **a** NP and **b** rayon fiber suspensions with different mass concentrations at 660 nm wavelength

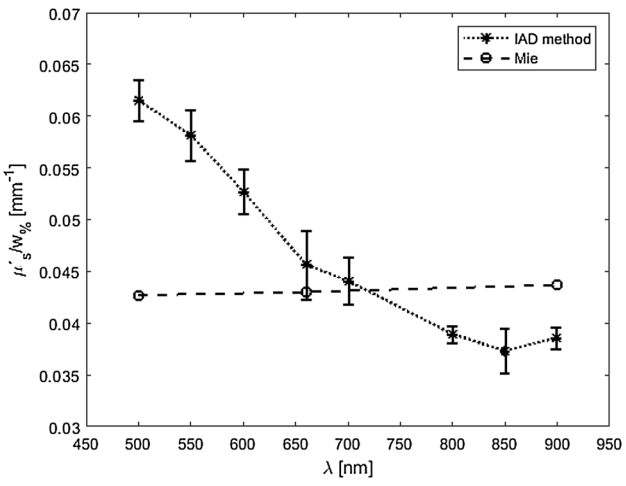

Fig. 7 Reduced scattering coefficient per mass concentration of NP fiber suspension measured with IAD method and calculated with Mie scattering

be considered to be negligible, since even bleached fibers have noticeable absorption due to cellulose and hemicellulose molecules [28]. High absorption is not necessarily problem for IAD method and it might, in some cases, even increase the convergence rate of IAD calculations due to stronger interaction with fibers. Laser backscattering analysis, on the other hand, has underlying theoretical assumption of $\mu_s' \gg \mu_a$ which may break at UV wavelengths or when unbleached fibers are examined and lignin is present. Outside the measured spectrum also water becomes remarkably absorptive.

5 Conclusion

We measured the reduced scattering coefficient of both deformed natural and nearly perfectly cylindrical artificial weakly absorbing fibers with two independent measurements and compared the results with Mie calculations based on an ideal cylinder model and combined with the measured size distribution of fibers. The possible effects of planar orientation of fibers on scattering measurements were eliminated in our experiments with two independent measurements where one was probing very large and turbulent measurement volume. While it is known that single fibers are not ideal scatterers, our measurements show that simple scattering model holds true for an ensemble of fibers if their size distribution is known. This is important as many industrial measurements based on the scattering of light are non-linear by nature and can be affected in poorly predictable manner by changes in fiber morphology. While our experiments were limited to pure fibers with no fillers or fines and no fibrillation, these can be taken into account as separate scatterers which obey their own size distribution and number density. Results also indicate that qualitative morphological data could be used to improve optical quantitative measurements if available.

Acknowledgements Open access funding provided by University of Oulu including Oulu University Hospital.

Compliance with ethical standards

Conflict of interest The authors declare that they have no conflict of interest.

References

1. Liptak, B.G.: Instrument Engineers' Handbook, Volume One: Process Measurement and Analysis, 4th edn. CRC Press, Boca Raton (2003)
2. Nakayama, S.: Microwave measurements of low pulp concentration in papermaking process. Jpn. J. Appl. Phys. **33**, 3614 (1994)
3. Nyfors, E.: Industrial microwave sensors? A review. Subsurf. Sens. Technol. Appl. **1**(1), 23–43 (2000)
4. Derakhshandeh, B., Kerekes, R.J., Hatzikiriakos, S.G., Bennington, C.P.J.: Rheology of pulp fibre suspensions: a critical review. Chem. Eng. Sci. **66**(15), 3460–3470 (2011)
5. Törmänen, M., Niemi, J., Löfqvist, T., Myllylä, R.: Pulp consistency determined by a combination of optical and acoustical measurement techniques. Meas. Sci. Technol. **17**(4), 695 (2006)
6. Törmänen, M., Myllylä, R.: Backward-mode photoacoustic transducer for sensing optical scattering and ultrasonic attenuation: determining fraction consistencies in pulp suspensions. Meas. Sci. Technol. **21**(2), 025105 (2010)
7. Saarinen, K., Muinonen, K.: Light scattering by wood fibers. Appl. Opt. **40**(28), 5064–5077 (2001)
8. International Organization for Standardization (2009) Particle size analysis—laser diffraction methods. Standard ISO 13320 (2009)
9. He, H., Zeng, N., Liao, R., Yun, T., Li, W., He, Y., Ma, H.: Application of sphere–cylinder scattering model to skeletal muscle. Opt. Express **18**, 15104 (2010)
10. Maeda, T., Arakawa, N., Takahashi, M., Aizu, Y.: Monte Carlo simulation of spectral reflectance using a multilayered skin tissue model. Opt. Rev. **17**(3), 223–229 (2010)
11. Linder, T., Löfqvist, T.: Monte Carlo simulation of photon transport in a randomly oriented sphere–cylinder scattering medium. Appl. Phys. B **105**, 659 (2011)
12. Linder, T., Löfqvist, T., Wernersson, E.L.G., Gren, P.: Light scattering in fibrous media with different degrees of in-plane fiber alignment. Opt. Express **22**(14), 16829–16840 (2014)
13. Bohren, C.F., Huffman, D.R.: Absorption and Scattering of Light by Small Particles. Wiley, New York (1983)
14. Hoosmüller, H., Sorensen, C.M.: Small and large particle limits of single scattering albedo for homogeneous spherical particles. J. Quant. Spectrosc. Radiat. Trans. **204**, 250 (2018)
15. Purcell, E.M., Pennypacker, C.R.: Scattering and absorption of light by nonspherical dielectric grains. Astrophys. J. **186**, 705 (1973)
16. Okamoto, H.: Light scattering by clusters: the A1-term method. Opt. Rev. **2**(6), 407–412 (1995)
17. Waterman, P.C.: Matrix formulation of electromagnetic scattering. Proc. IEEE **53**(8), 805 (1965). https://doi.org/10.1109/PROC.1965.4058
18. Schäfer, J.: Implementierung und anwendung analytischer und numerischer verfahren zur lösung der maxwellgleichungen für die untersuchung der lichtausbreitung in biologischem gewebe. Ph.D. thesis (2011)
19. Schäfer, J., Lee, S.C., Kienle, A.: Calculation of the near fields for the scattering of electromagnetic waves by multiple infinite cylinders at perpendicular incidence. J. Quant. Spectrosc. Radiat. Trans. **113**(16), 2113 (2012)

20. Prahl, S.A., van Gemert, M.J.C., Welch, A.J.: Determining the optical properties of turbid media by using the adding doubling method. Appl. Opt. **32**, 559 (1993)
21. Prahl, S.A.: Inverse adding–doubling software. https://omlc.org/software/iad/index.html. Accessed 26 Feb 2019
22. Juttula, H.J., Kananen, T.P., Mäkynen, A.J.: Instrument for measurement of optical parameters of turbid media by using diffuse reflectance of laser with oblique incidence angle. IEEE Trans. Instrum. Meas. **63**, 1301 (2014)
23. Lin, S.P., Wang, L., Jacques, S.L., Tittel, F.K.: Measurement of tissue optical properties by the use of oblique-incidence optical fiber reflectometry. Appl. Opt. **36**(1), 136–143 (1997)
24. Daimon, M., Masumura, A.: Measurement of the refractive index of distilled water from the near-infrared region to the ultraviolet region. Appl. Opt. **46**, 3811 (2007)
25. Juttula, H., Mäkynen, A.J.: Determination of refractive index of softwood using immersion liquid method. In: 2012 IEEE International Instrumentation and Measurement Technology Conference Proceedings. pp. 1231–1234 (2012). https://doi.org/10.1109/I2MTC.2012.6229360
26. Kasarova, S.N., Sultanova, N.G., Ivanov, C.D., Nikolov, I.D.: Analysis of the dispersion of optical plastic materials. Opt. Mater. **29**, 1481 (2007)
27. Keränen, V.T.J., Mäkynen, A.J., Prahl, S.A., Törmanen, M.: A scattering measurement system to determine the optical characteristics of industrial suspensions. In: 2009 IEEE instrumentation and measurement technology conference, pp. 570–573 (2009). https://doi.org/10.1109/IMTC.2009.5168515
28. Feng, Y., Zhang, J., He, J., Zhang, J.: Transparent cellulose/polyhedral oligomeric silsesquioxane nanocomposites with enhanced UV-shielding properties. Carbohydr. Polym. **147**, 171 (2016)